



Research Article

<https://doi.org/10.1631/jzus.A2500676>

Mechanical degradation characterization in remolded moraine soils and microstructure evolution under freeze–thaw cycles

Tuo LU^{1,2,3,4}, Yongbo TIE^{1,2,3}✉, Sai K. VANAPALLI⁴, Zhaoyu LI^{1,2}

¹Chinese Academy of Geological Sciences, Beijing 100037, China

²Chengdu Center of China Geological Survey, Chengdu 610081, China

³School of Engineering and Technology, China University of Geosciences, Beijing 100083, China

⁴Department of Civil Engineering, University of Ottawa, Ottawa K1N 6N5, Canada

Abstract: Remolded moraine soils are highly susceptible to degradation caused by freeze–thaw (F-T) cycles, posing significant risks to the stability of slopes in hilly regions. This study investigates the mechanical degradation and microstructural changes induced by F-T cycles through a comprehensive experimental program, including F-T cycle tests, triaxial shear tests (TSTs), unconfined compression tests (UCTs), and micro-CT scanning of moraine soil from southeast Xizang. The results reveal three stages of mechanical parameter degradation: rapid decline, moderate reduction, and plateau. Cohesion, initial average elastic modulus, and strength decrease significantly under low confining pressure (40~50% reduction), while the decrease is less pronounced under higher pressures (30~10%). Micro-CT scanning shows a clear evolution in the microstructure, with the porosity increasing from 14.25% to 18.69% and the pore-crack size rising from 69.83 μm to 90.44 μm . These microstructural changes are identified as the primary mechanism behind macroscopic degradation. A novel gray model (LGM) was developed to predict mechanical parameter evolution, showing high accuracy for predicting the strength of moraine soils in later F-T cycles (e.g., 15th, 20th, and beyond). The LGM model provides valuable insights for the design of moraine slopes and infrastructure subjected to freeze–thaw conditions.

Key words: Moraine soils; Freeze–thaw cycles; Mechanical degradation; Micro-CT; Gray models

1 Introduction

With the advancement of key national strategies such as China's Western Development, the Belt and Road Initiative, and the ongoing development of critical railways and highways, addressing the challenges posed by frost damage in cold regions has become increasingly crucial (Li et al., 2022; Zeng et al., 2024). Freeze–thaw (F-T) cycles in high-altitude mountainous areas are a significant factor both with respect to engineering safety and soil erosion processes in moraine soils (Wu et al., 2010; Fan et al., 2023).

Moraine soils, formed by the deposition and transport of sediments by glaciers, are widely distributed in Xizang. These soils are primarily sandy or gravelly, with significant proportions of silt and clay content (Jiang et al., 2020; Li, et al., 2022; Lu et al., 2025).

Numerous geohazards that include landslides, glacial lake outburst floods, and glacial debris flows during the past decade involving moraine soils are partly attributed to the influence of repeated F-T cycles in various regions of the world, including Alaska, Greenland, northern Canada, Russia, and Xizang (Emmer et al., 2020; Rechberger et al., 2021; Allen et al., 2022; Wang et al., 2024). Most of these geohazards arise due to the degradation of the mechanical properties of moraine soils and glacial tills (Cui et al., 2013; Chen et al., 2019). In recent years, some researchers have focused on the mechanical behavior of (remolded) moraine soils. Some studies have shown that the shear strength of

✉ Yongbo TIE, tyongbo@mail.cgs.gov.cn

Yongbo TIE, <https://orcid.org/0000-0001-7241-2942>

Tuo LU, <https://orcid.org/0000-0001-6019-188X>

Sai K. VANAPALLI, <https://orcid.org/0000-0002-3273-6149>

moraine soils significantly decreases with increasing degree of saturation or water content (Winter, 2004; Han et al., 2016; Vanapalli and Han, 2016; Zhou et al., 2019). Several studies have investigated remolded moraine soils with a relative density greater than 70%, which exhibit significantly higher shear strength (Jiang et al., 2024b; Zeng, et al., 2024). Some studies suggest that uniaxial compressive and triaxial shear strength decrease substantially with increasing F-T cycles, with cohesion showing an exponential decline (Chen et al., 2024; Jiang et al., 2024a; Jinke et al., 2024). Additionally, Mingli et al. (2025) conducted numerical simulations to assess mechanical damage in remolded moraine soils subjected to F-T cycles using the discrete element method (DEM). However, there is a lack of mathematical equations describing the degradation of mechanical parameters in (remolded) moraine soils under F-T cycles. Furthermore, the evolution of the 3D pore-crack structure in moraine soils under F-T cycles was hardly revealed.

Several researchers in recent years have used X-ray computed tomography (CT), known for its nondestructive nature and high resolution, to characterize the 3D microstructural features of soils (Yu et al., 2024) Hence, X-ray CT can be a valuable tool for quantifying the development of pores and cracks during F-T cycles, offering new insights into the micromechanisms that drive strength deterioration in (remolded) moraine soils.

This study explores the mechanical deterioration of (remolded) moraine soils subjected to F-T cycles through triaxial shear tests (TSTs) and unconfined compression tests (UCTs). X-ray CT and deep learning technology were employed to characterize the microstructure and evolution of pore cracks during F-T cycles. Furthermore, a new gray model (LGM) was developed to fit and predict the key mechanical strength parameters of moraine soils (e.g., shear strength, cohesion, and initial average elastic modulus) under F-T cycles.

2 Materials and methods

2.1 Investigation and sampling

This study site (longitude: 94.74557584, latitude: 29.48186613, WGS-84) is located along the lower Yarlung Tsangpo River in southeastern Xizang and is

characterized by a monsoon maritime climate, with precipitation primarily concentrated in the summer. It is characterized by marine-type glaciers influenced by moist airflows from the Indian Ocean, which can be classified as a seasonally frozen terrain. Moraine soils and glacial tills are widely distributed in the southeastern region of Xizang, with a notable concentration extending from Bomi County to Milin County in Linzhi city (Li, et al., 2022).

Fig. 1 illustrates the details of the glacial and moraine surface survey, as well as some tests conducted in this study. Moraine soil was collected from Danniang Town, Milin County (at 2970 m).

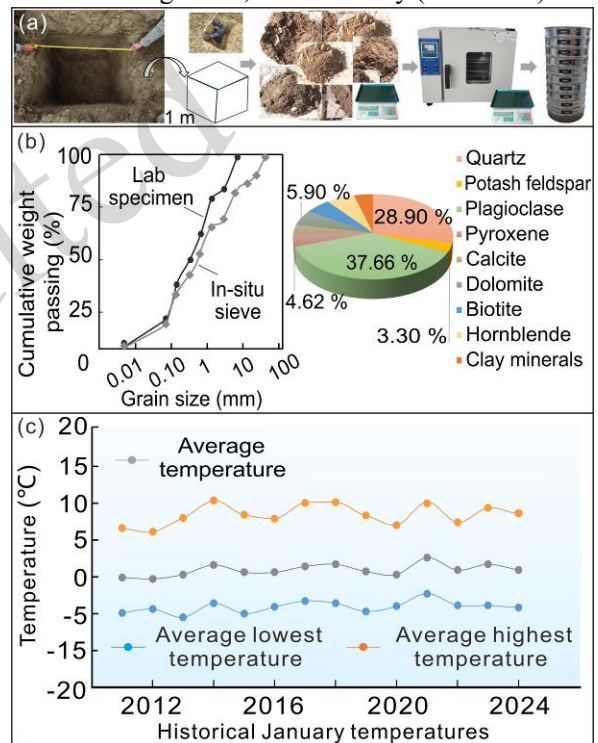


Fig. 1 Study area and sampling. (a) Representative soil sample collection from a test pit of 1 m depth for performing various tests. (b) Grain size analysis results and mineral composition. (c) January information of Milin County (<http://data.cma.cn/>).

Fig. 1(a) and (b) show the sieve analysis equipment and the grain size distribution (GSD) results, respectively. The GSD reveals a composition of 10.35% fine grains (<0.075 mm), 51.87% sand (0.075-2 mm), and 37.78% gravel (2-60 mm). X-ray diffraction (XRD) was employed to identify the mineral components in the soil; the major minerals identified included quartz, plagioclase, hornblende, dolomite, calcite, and various clay minerals (Fig.

1(b)). Notably, quartz and plagioclase constitute significant proportions of this mineral assemblage, at approximately 28.9% and 37.7%, respectively.

The moraine soil in the study area is classified as unconsolidated and exhibits a loose structure. Due to the lack of cementation, collecting undisturbed field samples is challenging, as the soil crumbles easily with minimal disturbance. The similarity ratio method is often employed to prepare remolded samples, where the soil is remixed and compacted to match the engineering properties of undisturbed soils as closely as possible (Feng et al., 2008). To address this, in this study, a remolded sample approach is extended for preparing specimens with comparable characteristics to overcome the lack of natural cementation and ensure consistency in sample structure for subsequent analysis (Table 1).

2.2 F-T cycles and mechanical tests

Table 1 presents the basic physical properties of the moraine soils. The moisture content of in situ moraine soils varies from 2.20% to 9.69%. The plastic and liquid limits are 15.1% and 21.6%, respectively. The dry density is approximately 1.90~2.0 g/cm³. The specific gravity is 2.66.

The initial moisture content of the remolded moraine soil specimens was controlled during specimen preparation (Fig. 2(a)). First, a predetermined mass of oven-dried particles was weighed (removing ≥ 10 mm particles because the maximum particle size should be smaller than 1/6~1/10 the diameter of the specimen, GB/T 50123-2019, ASTM D3080), and the required amount of deionized water was calculated according to the target moisture content. Both the in-situ gradation curve and the lab gradation curve after particle removal are shown in Fig. 1(c). Deionized water was gradually sprayed onto the soil using a fine-mist sprayer while the soil was continuously mixed to promote uniform water distribution. During this process, the wetted soil mass was repeatedly weighed to ensure that the target moisture content was achieved. After that, the compaction process was carried out in five equal layers, with each layer carefully placed and compacted to ensure uniform density distribution throughout the specimen height (cylindrical specimens: 61.8 mm in diameter and 125 mm in height). The wetted specimen soil was sealed

and stored for 24 h to allow moisture equilibration. In addition, specimens with a gravel fraction (> 2 mm) less than 40% by mass were tested using a conventional triaxial or direct shear apparatus to measure mechanical properties (GB/T 50123-2019, ASTM D3080).

During the freeze–thaw cycle tests, each compacted specimen was tightly wrapped with plastic film and then placed in a small box and sealed. This combined sealing method was used to minimize moisture exchange between the specimen and the external environment. The specimens were weighed before and after freeze–thaw cycles to check possible moisture variation. The weighing results indicated that moisture loss during freeze–thaw cycling was very limited. Therefore, no additional water was supplied during the freeze–thaw process, and the tests were conducted under sealed, relatively closed moisture conditions.

Table 1 Physical properties of remolded moraine soils

G_s	ρ_d (g/cm ³)	e	ω_0 (%)	Filed grain size scale (mm)	Grain size scale in test (mm)
2.66	1.9	0.40	10.0	0.001~60	0.001~10

G_s —Specific gravity, ρ_d —Dry density, e —Void ratio, ω_0 —Water content in test.

Over the past decade, January has been the coldest month in this region's winter conditions, characterized by semiarid conditions with minimal precipitation and an average temperature of 0.9 °C. The average lowest temperature in January ranges from -2.3 °C to -5.5 °C (Fig. 1(f)), while the average highest temperature ranges from 6.1 °C to 9.6 °C. Nighttime durations generally exceed 12 hours, while daytime durations are shorter. Consequently, the freezing temperature and duration were set at -6.0 °C and 13 hours, respectively, in this study. At this temperature, -6 °C is sufficient to freeze the pore water within moraine soils (Wei et al., 2025). Subsequently, thawing was conducted at 10.0 °C for 11 hours. This entire process was considered one freeze–thaw (F-T) cycle (Fig. 2(b)). Several studies suggest that most degradation of mechanical properties occurs during the 20 F-T cycles (Jiang, et al., 2024a; Jinke, et al., 2024; Qiu et al., 2024). Hence,

0, 2, 5, 10, 15, and 20 cycles were applied to the specimens in a temperature-controlled freezing-thaw device (error ± 0.5 °C).

As shown in Fig. 2(c), the specimens' mechanical properties were measured via unconfined compression tests (UCT; loading rate = 1.0 mm/min; maximum axial force capacity = 7.5 kN) and conventional unconsolidated undrained (UU) triaxial shear tests (TST; loading rate = 0.8 mm/min; maximum axial force capacity = 100 kN).

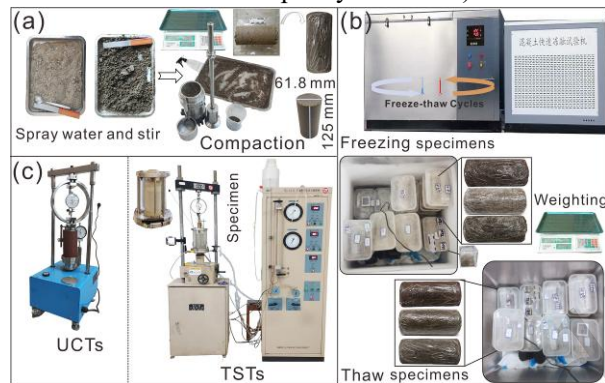


Fig. 2 F-T cycles and mechanical tests. (a) Remolded specimen preparation. (b) F-T cycles. (c) UCT and TST.

2.3 Micro-CT scanning

For the micro-CT scanning tests, irregular sub-specimens (SS1, SS2, and SS3) were carefully selected from the central part of the corresponding large cylindrical specimens without F-T cycles (Fig. 3(a1)). SS3 was applied in the mercury intrusion porosimetry (MIP) test (Micro Active AutoPore V9600 device, equipped with a large dilatometer). The MIP results revealed the pore size distribution across a broader range, including the micropores, which were less well captured by micro-CT.

This selection strategy was adopted to reduce possible boundary effects caused by specimen preparation and surface disturbance. The selected sub-specimens had no visible cracks or artificial damage caused by cutting or handling, and had comparable sizes suitable for micro-CT scanning. Therefore, although the micro-CT specimens were irregular in shape, they were considered representative of the internal microstructural characteristics of the corresponding F-T cycle specimens. To improve the comparability of the micro-CT results, all selected specimens were scanned under the same scanning parameters, and the reconstructed images were processed using the same

region-of-interest selection, deep learning model, and pore-structure analysis procedure. Three irregular sub-specimens were prepared for micro-CT scanning by placing them in a container with approximate dimensions of 15 mm \times 15 mm \times 15 mm (Figs. 3(a-b)).

Micro-CT scanning was performed using the Xradia 520 Versa system manufactured by Zeiss, Germany. The scanning resolution was 8.0 μ m per pixel, with a maximum scanning volume of 10 mm in width and height. Each scan produced approximately 1,200 slice images of raw data (1700 \times 1700 pixels per slice \times 1200 slices, 16-bit grayscale). The operating voltage and current were set to 50 kV and 81 μ A, respectively (Fig. 3(a2)). The initial micro-CT images were first preprocessed to enhance image quality and prepare them for subsequent analysis. A nonlocal means filter was applied to suppress noise while preserving edge details. The filtered images were then cropped to a uniform resolution of 1024 pixels \times 1024 pixels \times 800 slices, and the grayscale range was normalized to [0-255], ensuring consistent data dimensions across all sub-specimens (Fig. 3(a3)).

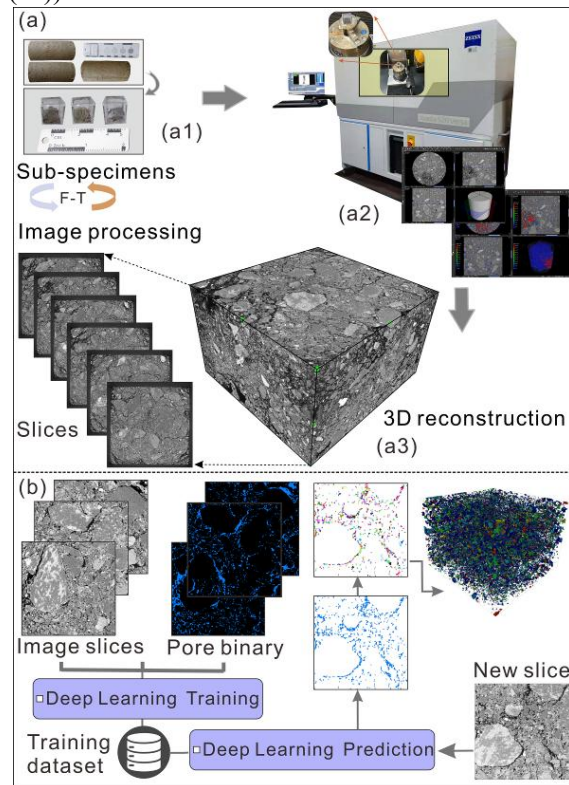


Fig. 3 Micro-CT scanning and image procedure. (a) Micro-CT scanning. (b) Deep learning segmentation of pore cracks.

To identify and quantify pore-crack and grain structures in remolded moraine soils, an enhanced U-Net convolutional neural network was employed (Ronneberger et al., 2015; Alom et al., 2019; Minaee et al., 2022). The U-Net model performs pixel-level semantic segmentation of CT images by learning multiscale features of fractures through deep convolutional and deconvolutional layers. This deep learning-based segmentation was implemented in MATLAB or AVIZO, leveraging the platforms' capabilities for deep learning model development and visualization of three-dimensional structures. MATLAB was used to train and test the network, and AVIZO was used for three-dimensional image processing and feature visualization. The micro-CT image dataset comprises 12,000 CT images, divided into a test set (containing 8,000 images) and a training set (containing 4,000 images) (Fig. 3(b)). The training images have a resolution of 1024×1024 pixels. They are specifically designed to focus on the analysis of pore cracks. When using the U-Net network algorithm for training (Liu et al., 2024), the batch size is set to 64, the epoch is set to 1000, and the learning rate is set to 0.0001.

Based on the separation results, several microstructural parameters were extracted from 3D CT images to describe the geometric characteristics of pore-crack networks, including porosity, pore size, and fractal dimension (Wei et al., 2020; Lu et al., 2023; Liu, et al., 2024).

(1) The three-dimensional (3D) porosity is the ratio of pore-crack voxels to the total number of voxels within the analyzed volume.

(2) The equivalent pore width (W_{EqW}) is defined based on the volume of the pore or crack and is calculated as follows:

$$W_{\text{EqW}} = \sqrt{\frac{4V}{\pi \cdot L}} \quad (1)$$

where L is the longest Feret diameter of the pore-crack. V is the pore-crack volume.

(3) The fractal dimension (D_v) is calculated as follows:

$$D_v = \frac{\ln(\delta)}{\ln(N(\delta))} \quad (2)$$

where δ represents the size of the measuring voxel box, and $N(\delta)$ is the number of boxes of size δ

required to cover the connected pore cracks.

3 A new gray model (LGM)

Several key mechanical parameters, including strength— q (triaxial shear strength (q_t), unconfined compression strength (q_u)) (Fig. 4(a)), initial average elastic modulus (E_0), and cohesion (c), were selected to evaluate the mechanical degradation behavior of remolded moraine soils under F-T cycles. In addition, the F-T cycle deterioration rate, K_{1-3} , for the deterioration of moraine soil mechanics is summarized below:

$$\begin{cases} K_1 = 1 - \frac{E_0(N)}{E_0(0)} \\ K_2 = 1 - \frac{q(N)}{q(0)} \\ K_3 = 1 - \frac{c(N)}{c(0)} \end{cases} \Rightarrow \begin{cases} K_1^* \\ K_2^* \end{cases} \quad (3)$$

where $E_0(0)$, $q(0)$, and $c(0)$ are the zero F-T cycle initial elastic modulus, strength (triaxial shear strength (q_t), unconfined compression strength (q_u)), and cohesion, respectively. $E_0(N)$, $q(N)$, and $c(N)$ are the N cycle values.

The mechanical degradation behavior of soils subjected to F-T cycles generally exhibits a nonlinear trend, which can be categorized into three distinct stages (Fig. 4(b)): an early stage with rapid strength loss, a middle stage with a decelerated degradation rate, and the end stage where the strength tends to stabilize and no longer change significantly (Chen, et al., 2024; Jiang, et al., 2024a; Jinke, et al., 2024; Qiu, et al., 2024).

A gray differential model (Equation (4)) is proposed to capture the degradation pattern of remolded moraine soils. This model allows the formulation of a differential equation where the degradation rate of mechanical parameters is expressed as a function of the number of F-T cycles. If the observed mechanical parameters after N freeze–thaw (F-T) cycles are denoted as a time series: $x = \{x(0), x(1), \dots, x(N)\}$, where x represents the initial average elastic modulus (E_0), strength (q_t or q_u) (Fig. 4(a)), or cohesion (c). The first-order difference $x^{(1)}$ is obtained by subtracting adjacent values in the sequence.

$$\Delta x = \{x(1) - x(0), x(2) - x(1), \dots, x(N) - x(N-1)\} \approx dx \quad (4)$$

A nonlinear gray differential model is then assumed in the form of:

$$\begin{cases} x = \frac{dx}{dN} = \lambda_1(x-H)^{\lambda_2}, \lambda_1 < 0, \lambda_2 > 1 \\ H = (1-K^*) \cdot x(0) \end{cases} \quad (5)$$

where $dx^{(0)}/dN$ denotes the change rate of the mechanical parameter $x^{(0)}$ concerning F-T cycles, λ_1 and λ_2 are autofitting parameters, and H is a horizontal asymptote representing the deterioration limit for estimating the ultimate value of strength after long F-T cycles. The parameter H can be calculated based on the F-T cycle deterioration rate $K_1 \sim K_2$. The parameters K^* are the empirical or experimentally measured maximum deterioration rate K_1^* or K_2^* , according to K_{1-2} (Equation (3)).

Taking the limits of Equation (5) under the conditions $x \rightarrow H$ and $x > H$, we obtain:

$$\begin{aligned} \lim_{\substack{N \rightarrow +\infty \\ x \rightarrow H}} (\lambda_1(x-H)^{\lambda_2}) &= 0 \\ \lim_{\substack{N \rightarrow 0^+ \\ x > H}} (\lambda_1(x-H)^{\lambda_2}) &= \lambda_1[x(0)-H]^{\lambda_2} \end{aligned} \quad (6)$$

This implies that as x approaches H and N approaches $+\infty$, the rate of change asymptotically tends to zero, indicating stabilization in the degradation process (see Fig. 4(b)).

Next, this study solves Equation (5):

$$\int \frac{1}{(x-H)^{\lambda_2}} dx = \int \lambda_1 dN \quad (7)$$

$$x(N) = H + \left[(1-\lambda_2)(\lambda_1 N + C) \right]^{\frac{1}{1-\lambda_2}} \quad (8)$$

Substitute $x(0)$ into Equation (8) to calculate C and $x(N)$.

$$C = \frac{(x(0)-H)^{1-\lambda_2}}{1-\lambda_2} \quad (9)$$

$$\begin{aligned} x(N) &= H + \left[(1-\lambda_2) \left(\lambda_1 N + \frac{(1-H)^{1-\lambda_2}}{1-\lambda_2} \right) \right]^{\frac{1}{1-\lambda_2}} \\ H &= (1-K^*) \cdot x(0), \lambda_1 > 0, \lambda_2 < 1 \end{aligned} \quad (10)$$

where the parameter H is the residual value after an

infinite number of freeze-thaw cycles (i.e., the long-term stabilized value). $x(0)$ is the initial value. The parameters K^* are the empirical or experimentally measured maximum deterioration rate K_1^* or K_2^* , according to K_{1-2} (Equation (3)).

Equations (10) and (5) are also named the Lu Gray Model (LGM), and the MATLAB code can be found at <https://github.com/LuTuo123/LGM>.

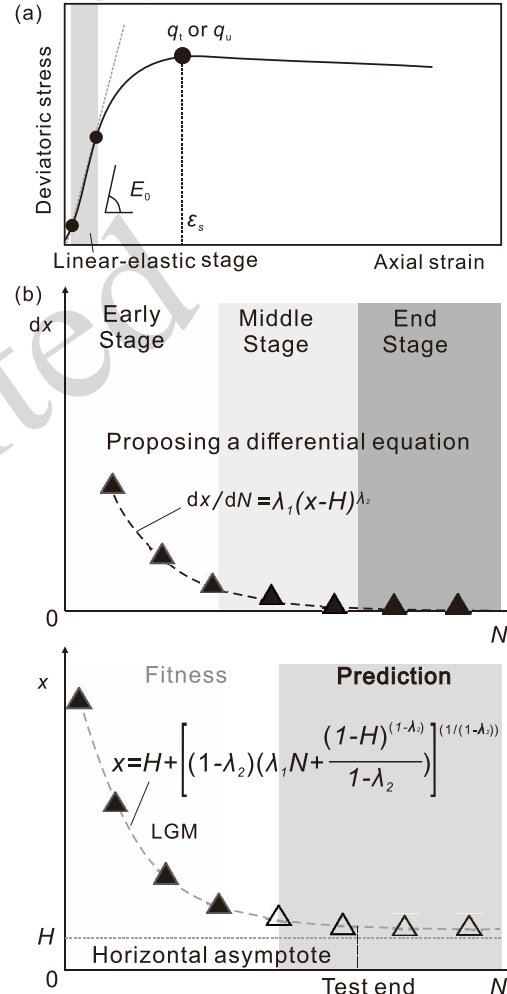


Fig. 4 A new gray model (LGM). (a) Mechanical parameters. (b) Gray differential equation and LGM (MATLAB code seen at <https://github.com/LuTuo123/LGM>).

The new model parameters λ_1 and λ_2 were estimated via nonlinear least squares fitting using the `lsqcurvefit` function. In this model, H denotes the residual value asymptotically approached by the soil after prolonged freeze-thaw cycles. The model remains applicable even when limited information on mechanical properties is available. This technique provides a robust and data-efficient framework for

predicting the mechanical parameters of moraine soils for 10~20 F-T cycles using limited information from 0 to 10 F-T cycles.

Taking the limit as $N \rightarrow +\infty$:

$$\lim_{\substack{N \rightarrow +\infty \\ x \rightarrow H}} x(N) = H + \lim_{N \rightarrow +\infty} \left[\left((1 - \lambda_2) \left(\lambda_1 N + \frac{(1 - H)^{1 - \lambda_2}}{1 - \lambda_2} \right) \right)^{\frac{1}{1 - \lambda_2}} \right] = H + \frac{1}{(+\infty)^{\lambda_2 - 1}} = H$$

4 Results and discussion

4.1 Stress–strain curves

Fig. 5 demonstrates that the failure modes of the strain-softening behavior were predominantly characterized by swelling. As deviatoric stress continuously increased during loading, both sides of the specimens developed parabolic or hyperbolic bulges. Simultaneously, the volume of the specimens increased, contributing to the shear dilatancy effect. Furthermore, no distinct splits or continuous cracks were observed at angles of 40° to 50° throughout the specimens. F-T cycles led to increased transverse cracks and uneven swelling (Fig. 5). F-T cycles significantly enhance the extent and probability of plastic deformation in moraine soils.

In typical strain-softening behavior, specimens exhibit an obvious peak followed by a significant reduction in stress resistance as the soil is strained. The stress–strain curve remains stable and gradually decreases with increasing strain after the yield strain (ϵ_s). The q_u and q_t decrease with the F-T cycles, and the difference between the peak shear strength (q_u and q_t) and residual strength decreases. After 20 F-T cycles, the narrowest gap between the peak shear strength (q_t) and residual strength is attributed to the progressive degradation of the soil structure and the development of pore-crack networks, particularly under a confining pressure (σ_3) of 200 kPa (Fig. 5).

4.2 Mechanical deterioration under F-T cycles

In the unconfined compression test (UCT), the specimen's initial average elastic modulus (E_0) decreased from 3.20 MPa to 1.50 MPa as the number

of F-T cycles increased from 0 to 20. The strength (q_u) of the specimen decreased from 40.8 kPa to 24.08 kPa as the number of F-T cycles rose from 0 to 20. Under different confining pressures (σ_3), both the initial average elastic modulus (E_0) and the shear strength (q_t) showed a decreasing trend with increasing F-T cycles (Fig. 6(a)).

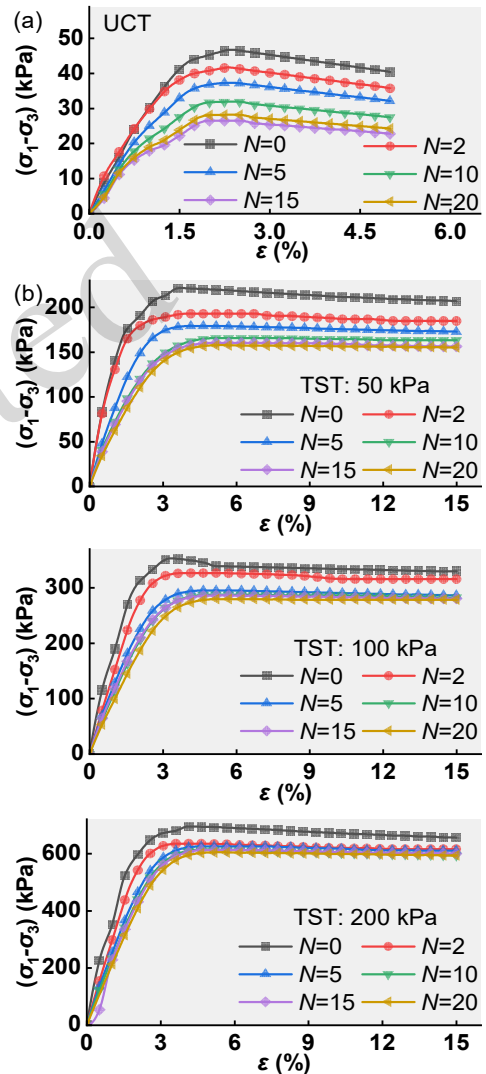


Fig. 5 The stress–strain curves. (a) UCT results. (b) TST results.

Under a confining pressure (σ_3) of 50 kPa, E_0 decreased from 14.24 MPa to 8.82 MPa, and q_t decreased from 202.07 kPa to 157.75 kPa. Under 100 kPa, E_0 declined from 20.09 MPa to 13.00 MPa, and q_t declined from 343.24 kPa to 279.93 kPa. Under 200 kPa, E_0 dropped from 36.12 MPa to 26.62 MPa, and q_t decreased from 674.24 kPa to 603.58 kPa. In

addition, the cohesion (c) sharply declined from 10.83 kPa to 6.50 kPa. The internal friction angle (φ) initially decreased and fluctuated, generally between 35° and 40° . This fluctuating (Jiang, et al., 2024a; Jinke, et al., 2024; Qiu, et al., 2024), decreasing trend indicates that the freeze–thaw cycle affects not only the bonding and cementation between particles but also the frictional resistance and interlocking behavior of the soil skeleton.

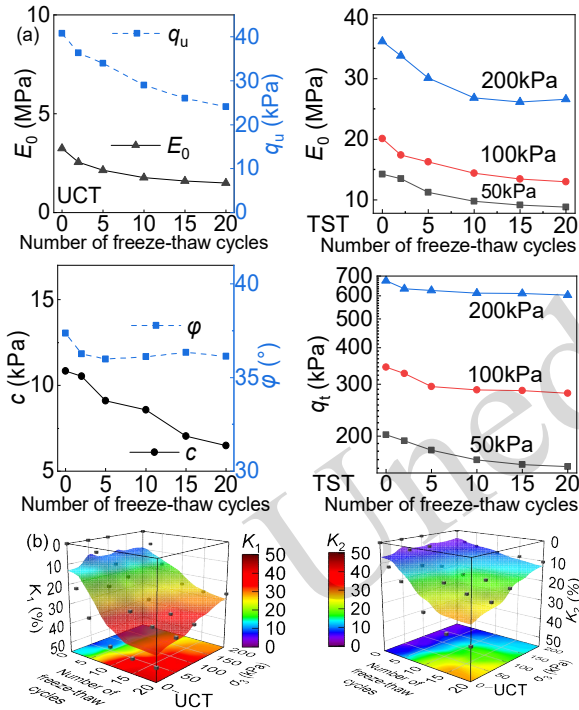


Fig. 6 F-T cycle mechanical deterioration. (a) Strength reduction. (b) F-T cycle deterioration rate, K_1 , and K_2 .

Specifically, in the UCT test, K_1 decreased by 47.91%, and K_2 decreased by 38.55%. At 50 kPa, K_1 declined to 38.03%, and K_2 declined to 21.94%. At 100 kPa, K_1 declined to 35.38%, and K_2 declined to 18.44%. At 200 kPa, K_1 was reduced to 26.31%, and K_2 was reduced to 10.48% (Fig. 6(b)).

4.3 Application of the new LGM

The predictive performance of the Lu-Gray model (LGM) was evaluated under different confining pressures and F-T cycles (Fig. 7(a), Table 2, and Table 3). Overall, the model consistently captures the attenuation trend of mechanical parameters with increasing F-T cycles ($R^2 > 0.96$). At confining pressures of 50, 100, and 200 kPa, the prediction lines

exhibit good agreement with the best-fit experimental data (relative error from -4.85% to 3.64%), particularly in describing the early and middle stages in F-T cycles. This observation confirms that the LGM approach is suitable for characterizing the nonlinear decay process of moraine soil strength parameters.

A similar trend is observed for q_u . The fitted curves reveal a pronounced reduction during the early stage of F-T cycles, followed by a transitional stage of moderate attenuation (middle stage) and finally a plateau stage where the values stabilize (end stage). The prediction curves successfully reproduce the degradation rate and the ultimate strength degradation in the middle-end stage (relative errors of -5.79% to -4.14%). Parameter H represents the ultimate value of the mechanical parameter degradation under F-T cycles.

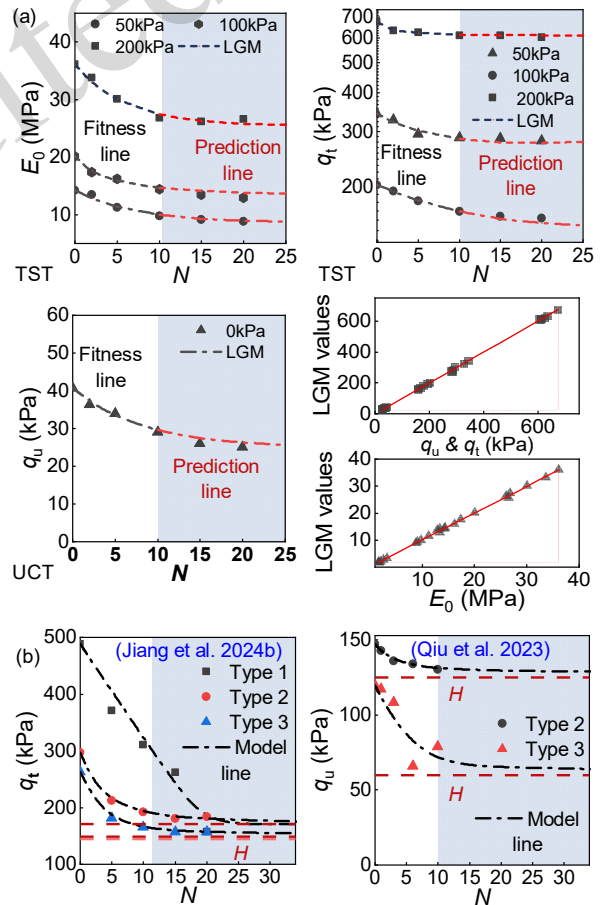


Fig. 7 LGM prediction. (a) The fitness and prediction results. (b) Application using data from Jiang et al. 2024b and Qiu et al. 2023. H denotes the ultimate value of strength degradation ($N \rightarrow \infty$).

Comparison with previous studies further

underscores the model's robustness. As shown in Fig. 7(b), the predicted results are comparable to those reported by Jiang et al. (2024b) and Qiu et al. (2023). In particular, the ultimate value (H) aligns closely with the literature, suggesting that the model can be applied across various soil types and testing conditions. In Jiang et al. (2024b), type 1 corresponds to moraine soil with a dry density of $2.0 \text{ g}\cdot\text{cm}^{-3}$ under a confining pressure of 200 kPa (CD test), type 2 corresponds to a dry density of $1.9 \text{ g}\cdot\text{cm}^{-3}$ under the

same conditions, and type 3 corresponds to a dry density of $1.8 \text{ g}\cdot\text{cm}^{-3}$ under 200 kPa (CD test). In Qiu et al. (2023), types 2 and 3 represent the UCT results of remolded moraine soil with gravel contents of 19.8%, 41.9%, and 53.9%, respectively.

This study has several limitations. The experimental tests were conducted with up to 20 freeze–thaw cycles, which is sufficient to capture the maximum degradation trends but may not fully reflect the long-term behavior of the soil.

Table 2 Fitness and prediction of E_0 results using LGM

σ_3 (kPa)	λ_1	λ_2	H (kPa)	R^2	K_1^* (%)	E_0 (MPa) ($N=15$)	Prediction (MPa)	Error (%)	E_0 (MPa) ($N=20$)	Prediction (MPa)	Error (%)
50	-0.13	1.01	8.54	0.96	40	9.11	9.26	-1.68	8.82	8.91	-0.95
100	0.00	1.58	13.06	0.98	35	13.42	14.05	-4.85	12.98	13.76	-2.15
200	-0.15	1.01	25.29	0.98	30	26.16	26.23	-0.27	26.62	25.71	3.41
0	-0.29	1.01	1.78	0.99	45	1.70	1.80	-5.61	1.69	1.79	-5.79

Table 3 Fitness and prediction of strength results using LGM

σ_3 (kPa)	λ_1	λ_2	H (kPa)	R^2	K_2^* (%)	q_t or q_u (kPa) ($N=15$)	Prediction (kPa)	Error (%)	q_t or q_u (kPa) ($N=20$)	Prediction (kPa)	Error (%)
50	-0.07	1.07	141.45	1.00	30	160.31	157.49	1.76	157.75	152.01	3.64
100	-0.18	1.01	274.59	0.97	20	285.94	276.19	3.41	279.93	274.85	1.82
200	-0.01	1.91	606.82	0.99	10	610.10	612.28	-0.36	603.58	610.92	-1.22
0	-0.10	1.10	24.48	0.98	40	26.05	27.24	-4.57	25.08	26.11	-4.14

The LGM model was used to predict mechanical properties beyond 20 cycles, but these predictions are extrapolated and have not been directly validated through long-term testing. The study focused on remolded moraine soil from a specific region, and the findings may not be directly applicable to other soil types or regions.

4.4 Microstructural deterioration

Fig. 4 shows the pore size ($>10 \mu\text{m}$) range captured by micro-CT and mercury intrusion porosimetry (MIP). This indicates that micro-CT can detect approximately half of the total porosity (Fig. 8(a)): the MIP-measured porosity is 28.95%. In contrast, micro-CT detects only 14.96% (the porosity of the representative subspecimen is 14.96%). This limitation arises from the resolution setting of the micro-CT scan (one voxel is $8.0 \mu\text{m}$ in this study). The three-dimensional pore-crack structure of moraine soils undergoes significant changes over time due to the influence of freeze–thaw (F-T) cycles (Fig. 8(b)). The microporosity exhibits a rapid initial

increase after 5 cycles. During the initial stage (0–5 cycles), the microporosity (SS1) ranged from 14.25% to 16.46%, reflecting an increase of approximately 15% to 50%. The average pore size (SS1) increased from $69.83 \mu\text{m}$ to $80.58 \mu\text{m}$, reflecting an increase of approximately 15% to 30%. This accelerating growth trend slowed in the subsequent cycles (10–20), with the microporosity of SS-1 ranging from 17.33% to 18.69%. The average pore size (SS1) increased from $80.58 \mu\text{m}$ to $90.44 \mu\text{m}$.

The freeze–thaw cycles significantly affect the shear strength and mechanical properties of moraine soils. One important aspect that is closely related to soil behavior under freeze–thaw conditions is the formation of shear bands. These localized zones of intense deformation play a crucial role in the mechanical degradation of soils during cyclic freeze–thaw processes (Wei et al., 2026). Shear bands not only influence the soil strength but also contribute to the localization of deformation, which in turn accelerates soil degradation. These findings are

consistent with the results of this study, where we observed that the mechanical degradation in moraine soils was largely controlled by the development of shear bands, which were observed to form progressively with increasing freeze–thaw cycles. The role of shear bands in the mechanical degradation mechanism of soil is critical to understanding how freeze–thaw cycles affect the long-term stability of moraine soils in real-world conditions.

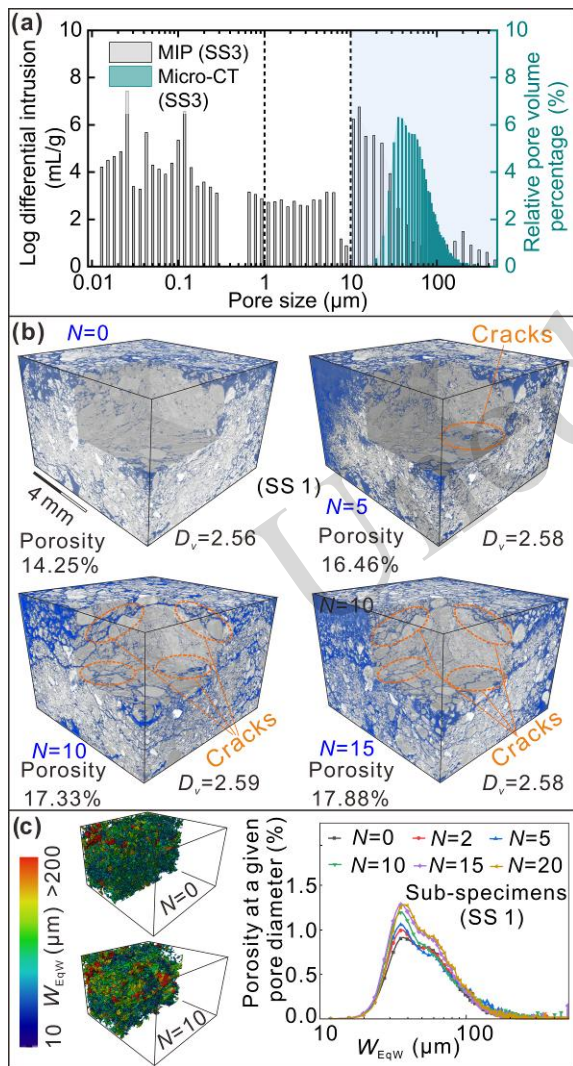


Fig. 8 Pore-crack evolution. (a) MIP vs. Micro-CT results; (b) The porosity. (c) Pore size distribution.

5 Conclusions

The mechanical degradation of remolded moraine soils subjected to different freeze–thaw (F-T) cycles was comprehensively investigated in this study,

including F-T cycle tests, triaxial shear tests, unconfined compression tests, and micro-CT scanning. Based on the results, a novel gray model (LGM) was developed to evaluate the mechanical degradation under F-T cycles. Key conclusions are summarized below:

(1) Three distinct stages of mechanical degradation: The mechanical strength of remolded moraine soils decreases significantly with increasing F-T cycles, showing three distinct stages: rapid decline, moderate reduction, and plateau, with parameters such as the initial average elastic modulus (E_0) and shear strength (q_t , q_u) following this three-stage degradation trend. Under a confining pressure of 0–50 kPa, the initial average elastic modulus and strength decrease by 40–50%, whereas at 100–200 kPa, the decrease is less severe (30–10%). Higher confining pressures help mitigate deterioration, likely due to partial crack closure.

(2) Key role of microstructural changes: Freeze–thaw cycles induce significant microstructural changes, primarily the initiation and propagation of pore-crack networks, leading to a 31% increase in porosity. The pore size distribution (PSD) shifts to larger sizes, with the average equivalent diameter (W_{EqW}) increasing from 69.83 μm to 90.44 μm and the microporosity increasing from 12.25% to 18.69%. These microstructural changes are critical in driving the observed mechanical degradation, as they coarsen the soil structure, reduce shear strength, and increase plastic deformation. At the shallow scale, F-T cycles accelerate microstructural deterioration, promoting preferential flow and further reducing shear strength, which makes the soil more prone to localized collapse under heavy rainfall.

(3) The contribution of the LGM model: The newly developed LGM model effectively captures the nonlinear deterioration of mechanical parameters, such as strength and elastic modulus, under F-T cycles. By calibrating experimental data from 0 to 10 F-T cycles, the model shows high predictive accuracy, with relative errors for strength predictions at the 15th and 20th cycles remaining below 6%. The LGM model not only fits the data from this study but has also been successfully applied to other studies, demonstrating its broad applicability. Importantly, the model’s ability to quantify strength degradation provides a reliable estimate of the long-term stability

threshold for moraine slopes and infrastructure.

Acknowledgments

The first author gratefully acknowledges and appreciates the China Scholarship Council and the University of Ottawa, Canada, for jointly funding his Ph.D. research program. This research work was supported by the National Natural Science Foundation of China (Grant No. U2544221), the Key Research and Development Program of Xizang Autonomous Region (Grant No. XZ202401ZY0029), and the Key Program of Natural Science Foundation of Xizang Autonomous Region (Grant No. XZ202401ZR0073).

Author contributions

Tuo Lu: Methodology, Conceptualization, Investigation, Programming, Analysis, Writing- original draft. Yongbo Tie: Supervision, conceptualization, writing-review & editing, funding acquisition. Sai Vanapalli: Supervision, Conceptualization, Methodology, Writing-review & editing. Zhaoyu Li: Investigation, Analysis, Data curation, Visualization.

Conflict of interest

The authors declare that they have no known competing financial interests or personal relationships that could have appeared to influence the work reported in this paper.

Declaration on the use of generative AI tools

We would like to clarify that AI tools were just utilized for grammar checking and academic language refinement of some sentences during the preparation of the manuscript.

Data availability

Data will be made available on request. The LGM MATLAB code is shown in <https://github.com/LuTuo123/LGM>

References

- Allen SK, Sattar A, King O, et al., 2022. Glacial lake outburst flood hazard under current and future conditions: Worst-case scenarios in a transboundary himalayan basin. *Nat. Hazards Earth Syst. Sci.*, 22(11):3765-3785. <https://doi.org/10.5194/nhess-22-3765-2022>
- Alom MZ, Taha TM, Yakopcic C, et al., 2019. A state-of-the-art survey on deep learning theory and architectures. *Electronics*, 8(3):292. <https://doi.org/10.3390/electronics8030292>
- Chen N, Wang Z, Tian S, et al., 2019. Study on debris flow process induced by moraine soil mass failure. *Quaternary Sciences*, 39(5):1235-1245. <https://doi.org/10.11928/j.issn.1001-7410.2019.05.15>
- Chen Z, Liu B, Liu Y, et al., 2024. Surrounding rock pressure in the tunnel portal section through moraine under freeze-thaw action. *Journal of Mountain Science*, 21(7):2480-2493. <https://doi.org/10.1007/s11629-023-8412-z>
- Cui P, Zou Q, Xiang L-Z, et al., 2013. Risk assessment of simultaneous debris flows in mountain townships. *Progress in Physical Geography: Earth and Environment*, 37(4):516-542. <https://doi.org/10.1177/0309133313491445>
- Emmer A, Klimeš J, Hölbling D, et al., 2020. Distinct types of landslides in moraines associated with the post-lia glacier thinning: Observations from the kinzl glacier, huascarán, peru. *Science of The Total Environment*, 739:139997. <https://doi.org/10.1016/j.scitotenv.2020.139997>
- Fan L, Zhong W, Wang G, et al., 2023. Optimal slag content for geopolymer composites under freeze-thaw cycles with different freezing temperatures. *Journal of Zhejiang University-SCIENCE A*, 24(4):366-376. <https://doi.org/10.1631/jzus.A2200437>
- Feng JD, Li JG, Wang R, et al., 2008. Large scale direct shear test on strength behavior of railway moraine soils in yunnan. *Yantu Lixue/Rock and Soil Mechanics*, 29(12):3205-3210. <https://doi.org/10.16285/j.rsm.2008.12.006>
- Han Z, Vanapalli SK, Kutlu ZN, 2016. Modeling behavior of friction pile in compacted glacial till. *International Journal of Geomechanics*, 16(6):D4016009. [https://doi.org/10.1061/\(ASCE\)GM.1943-5622.0000659](https://doi.org/10.1061/(ASCE)GM.1943-5622.0000659)
- Jiang H, Zheng G, Yi Y, et al., 2020. Progress and challenges in studying regional permafrost in the tibetan plateau using satellite remote sensing and models. *Frontiers in Earth Science*, 8. <https://doi.org/10.3389/feart.2020.560403>
- Jiang T, Pan H, Ai Y, 2024a. Effect of freeze-thaw cycles and water content on the mechanical properties of moraine soil. *Bulletin of Geological Science and Technology*, 43(2):238-252. <https://doi.org/10.19509/j.cnki.dzkq.tb20220649>
- Jiang Y, Lu X, Liu Z, et al., 2024b. Experimental study on the engineering properties and failure mechanism of moraine in southeast tibet under freeze-thaw cycles conditions. *Engineering Failure Analysis*, 163:108551. <https://doi.org/10.1016/j.engfailanal.2024.108551>
- Jinke F, Zurun Y, Zihao H, et al., 2024. Study on prediction model of strength deterioration of moraine soil under high frequency freeze-thaw cycles. *Journal of Glaciology and Geocryology*, 46(2):602-611. <https://doi.org/10.7522/j.issn.1000-0240.2024.0049>
- Li C, Wang R, Gu D, et al., 2022. Temperature and ice form effects on mechanical behaviors of ice-rich moraine soil of tianmo valley nearby the sichuan-tibet railway. *Engineering Geology*, 305:106713. <https://doi.org/10.1016/j.enggeo.2022.106713>
- Liu H, Dai X, Yang G, et al., 2024. Damage evolution characteristics of freeze-thaw rock combined with ct image and deep learning technology. *Bulletin of Engineering Geology and the Environment*, 84(1):20. <https://doi.org/10.1007/s10064-024-04010-3>
- Lu T, Tang Y, Tie Y, et al., 2023. Fractal analysis of small-micro pores and estimation of permeability of loess

- using mercury intrusion porosimetry. *Journal of Zhejiang University-SCIENCE A*, 24(7):584-595. <https://doi.org/10.1631/jzus.A2200528>
- Lu T, Tie Y, Song S, et al., 2025. Quantitative assessment of calcareous cementation in moraine soils: Insights from an integrated mineralogical and granulometric analysis. *Bulletin of Engineering Geology and the Environment*, 84(11):479. <https://doi.org/10.1007/s10064-025-04451-4>
- Minaee S, Boykov Y, Porikli F, et al., 2022. Image segmentation using deep learning: A survey. *IEEE Transactions on Pattern Analysis and Machine Intelligence*, 44(7):3523-3542. <https://doi.org/10.1109/TPAMI.2021.3059968>
- Mingli L, Jianuo L, Yuanjun J, et al., 2025. The study of microscopic damage in moraine soils under freeze-thaw cycles based on discrete element. *Bulletin of Engineering Geology and the Environment*, 84(11):558. <https://doi.org/10.1007/s10064-025-04606-3>
- Qiu E, Pan H, He Q, et al., 2024. Tests on the mechanical properties of moraine soils under freeze-thaw conditions and the modified duncan-chang model. *Journal of Engineering Geology*, 3:772-784. <https://doi.org/10.13544/j.cnki.jeg.2023-0351>
- Rechberger C, Fey C, Zangerl C, 2021. Structural characterisation, internal deformation, and kinematics of an active deep-seated rock slide in a valley glacier retreat area. *Engineering Geology*, 286:106048. <https://doi.org/10.1016/j.enggeo.2021.106048>
- Vanapalli SK, Han Z, 2016. Modelling the mechanical properties of a compacted glacial till. *Indian Geotechnical Journal*, 46(3):261-271. <https://doi.org/10.1007/s40098-016-0183-9>
- Wang R, Li C, Gu D, et al., 2024. Strength criterion of ice-rich moraine soil considering the ice form and temperature based on thermal-mechanical triaxial tests. *Cold Regions Science and Technology*, 220:104150. <https://doi.org/10.1016/j.coldregions.2024.104150>
- Wei X, Shen Y, Wei Z, et al., 2025. Resistivity and unfrozen water content of moraine soil at freezing temperatures: Experiments and thermodynamic modeling. *Cold Regions Science and Technology*, 235:104494. <https://doi.org/10.1016/j.coldregions.2025.104494>
- Wei X, Shen Y, Wang Y, et al., 2026. Shear behaviors of freeze-thaw interface in moraine soil: Experimental and theoretical approaches. *Journal of Rock Mechanics and Geotechnical Engineering*, <https://doi.org/10.1016/j.jrmge.2026.01.012>
- Wei Y-N, Fan W, Yu B, et al., 2020. Characterization and evolution of three-dimensional microstructure of malan loess. *Catena*, 192:104585. <https://doi.org/10.1016/j.catena.2020.104585>
- Winter MG, 2004. Determination of the acceptability of glacial tills for earthworks. *Quarterly Journal of Engineering Geology and Hydrogeology*, 37(3):187-204. <https://doi.org/10.1144/1470-9236/04-017>
- Wu Y-P, Guo J, Guo C-X, et al., 2010. Exothermic process of cast-in-place pile foundation and its thermal agitation of the frozen ground under a long dry bridge on the qinghai-tibet railway. *Journal of Zhejiang University SCIENCE A*, 11(2):88-96. <https://doi.org/10.1631/jzus.A0900522>
- Yu B, Dijkstra TA, Fan W, et al., 2024. Advanced multi-scale characterization of loess microstructure: Integrating μ xt and fib-sem for detailed fabric analysis and geotechnical implications. *Engineering Geology*, 341:107727. <https://doi.org/10.1016/j.enggeo.2024.107727>
- Zeng Z-X, Zhang L-M, Xu Z-D, et al., 2024. Mechanical behaviour and grain breakage characteristics of tibetan glacial tills under triaxial compression. *Acta Geotechnica*, 19:4809-4822. <https://doi.org/10.1007/s11440-023-02195-7>
- Zhou GGD, Chen L-L, Mu Q-Y, et al., 2019. Effects of water content on the shear behavior and critical state of glacial till in tianmo gully of tibet, china. *Journal of Mountain Science*, 16(8):1743-1759. <https://doi.org/10.1007/s11629-019-5440-9>

中文概要

题目: 冻融循环下(重塑)冰碛土力学性质与微观结构劣化特征

作者: 鲁拓^{1,2,3,4}, 铁永波^{1,2,3}, Sai K. VANAPALLI⁴, 李照宇^{1,2}

机构: ¹中国地质科学院, 中国北京, 100037; ²中国地质调查局成都地质调查中心(西南地质科技创新中心), 中国成都, 611734; ³中国地质大学(北京), 工程技术学院, 中国北京, 100083; ⁴渥太华大学, 工程学院土木工程系, 加拿大渥太华, K1N 6N5

目的: 本文旨在系统研究冻融循环对重塑冰碛土的力学性质劣化及其微观结构演化机制, 提出冻融作用下的冰碛土强度劣化数学方程。

创新点: 1. 提出了新型的 LGM 模型, 该模型能够有效捕捉冰碛土在冻融循环中的力学参数劣化规律。2. 通过微 CT 扫描技术, 揭示了冻融循环对冰碛土劣化的微观机制, 定量分析了孔隙率和平均孔径大小的变化及对宏观力学的影响。

方法: 1. 通过冻融循环试验、三轴剪切试验、无侧限压缩试验和 Micro-CT 扫描等综合实验手段, 详细研究了冻融循环对重塑冰碛土力学性能的影响(图 2 和图 3); 2. 运用 Micro-CT 扫描技术, 分析了冻融循环下冰碛土微观结构(如孔隙率和孔裂隙大小)的变化, 揭示

了微观结构变化如何驱动力学性能劣化（图8和图9）；3. 基于0至10次冻融循环数据，建立了LGM模型，并验证了该模型在第15次和第20次冻融循环中对强度参数等准确预测(公式5，公式10，图4，图11)。

结论：1. 本研究揭示了冰碛土在冻融循环中的力学劣化特征遵循三个阶段：快速下降、适度减少和平稳期。内聚力、初始弹性模量和剪切强度在低围压损失幅度较大（40~50%），而高围压下损失幅度较小（30~10%）；2. 冻融循环显著影响冰碛土的微观结构，孔隙率从14.25%增加到18.69%，平均孔径从69.83 μm 增加到90.44 μm 。微观结构变化是驱导致力学性能退化的主要机制；3. 基于0至10次冻融循环的实验数据，建立了LGM模型，并验证了该模型在第15次和第20次冻融循环中的强度，最大相对误差保持在6%以内。

关键词：冰碛土；冻融循环；力学劣化；Micro-CT；灰色模型